DISCLAIMER

This report was prepared as an account of work sponsored by an agency of the United States Government. Neither the United States Government nor any agency thereof, nor any of their employees, makes any warranty, express or implied, or assumes any legal liability or responsibility for the accuracy, completeness, or usefulness of any information, apparatus, product, or process disclosed, or represents that its use would not infringe privately owned rights. Reference herein to any specific commercial product, process, or service by trade name, trademark, manufacturer, or otherwise does not necessarily constitute or imply its endorsement, recommendation, or favoring by the United States Government or any agency thereof. The views and opinions of authors expressed herein do not necessarily state or reflect those of the United States Government or any agency thereof. Reference herein to any social initiative (including but not limited to Diversity, Equity, and Inclusion (DEI); Community Benefits Plans (CBP); Justice 40; etc.) is made by the Author independent of any current requirement by the United States Government and does not constitute or imply endorsement, recommendation, or support by the United States Government or any agency thereof.

Fermilab

Study and improvement of the trigger system in ICARUS

FERMILAB-TM-2872-STUDENT

Fermi National Accelerator Laboratory
Italian Student Program 2023

Study and improvement of the trigger system in ICARUS

Internship report

Giovanni Chiello

Under the supervision of Angela Fava and Donatella Torretta

Abstract In recent years, intriguing experimental neutrino anomalies have emerged. If confirmed, they could hint at the presence of additional sterile neutrino states playing in neutrino mixing. The Short-Baseline Neutrino project at Fermilab aims to delve into these anomalies, utilizing three Liquid Argon Time Projection Chamber detectors along the Booster Neutrino Beam. The SBND detector serves as nearby instruments, while MicroBooNE and ICARUS function as far detectors and also explore the NuMI beam off-axis.

A relevant aspect in the functioning of all SBN detectors is the trigger system, that determines which interactions are recorded. In particular, in ICARUS, it relies on the synchronization of prompt signals from scintillation light within the LAr-TPC, detected by a system of Photo-Multiplier Tubes, with the proton beam's spill extraction. The existing majority-based logic of the trigger system could potentially be enhanced through adder boards that sum analog signals from PMTs in groups of 15. This sum-based triggering might aid in identifying events near TPC walls, where light is abundant but captured by only a few PMTs, potentially bypassing the majority condition. Comprehensive tests have been performed to characterize these adder boards.

Keywords ICARUS; SBN; Neutrino; Trigger; Adder.

Contents

Giovanni Chiello
Università di Pisa
56126 Pisa, Italy
Tel.: (+39) 329 185 3148
E-mail: g.chiello@studenti.unipi.it

1 Introduction

The ICARUS T600 detector constitutes one of the trio of detectors within the SBN Program[1], standing as the pioneering large-scale LArTPC[2]. The next sections will delve into both the SBN Program and ICARUS itself, placing special emphasis on their physics objectives and the key attributes of the detector. [1]

1.1 The SBN Program

The Fermilab Short-Baseline Neutrino program was put forth in 2015 with the aim of providing a conclusive response and presenting an intriguing avenue for neutrino physics exploration. This encompasses the capacity to address a set of experimental anomalies on neutrino oscillations at short baseline and to conduct the most finely-tuned search to date for sterile neutrinos at the eV mass scale, spanning both ν_e appearance and ν_μ disappearance channels. [2]

It employs three detectors, based on the common technology of Liquid-Argon TPC: the first and the nearest one is SBND[3], located at 110 m from the BNB[4] target; the middle one is MicroBooNE[5], located at 470 m from the target in the LArTF[6]; the last and the furthest one is ICARUS[7], located at 600 m from the target. The selection of these sites was chosen to optimize the sensitivity to short-baseline neutrino oscillations, in the region of the parameter space where anomalies have been observed by LSND and MiniBooNE experiments. The use of one neutrino beam and the same detection technique allow to minimize systematic uncertainties related to neutrino flux, cross section and detector. [2] Layout and main detector features can be found in Fig. 1 and Table 1.

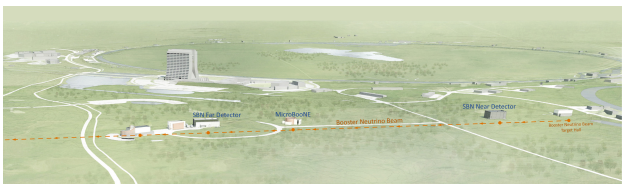

Fig. 1: SBN layout. It encompasses three LAr-TPC detectors aligned along the axis of the BNB. Starting from the right, we have SBND at 110 meters, followed by MicroBooNE at 470 meters and ICARUS at 600 meters.

[1] Short-Baseline Neutrino Program
[2] Liquid-Argon Time Projection Chamber
[3] Short-Baseline Near Detector
[4] Booster Neutrino Beam
[5] Micro Booster Neutrino Experiment
[6] Liquid-Argon Test Facility
[7] Imaging Cosmic And Rare Underground Signal

	Baseline	*Total LAr*	*Active LAr*
SBN-ND	110 m	220 t	112 t
MicroBooNE	470 m	170 t	89 t
ICARUS	600 m	760 t	476 t

Table 1: Summary of the main SBN detector features.

The Booster Neutrino Beam is produced by extracting protons with a kinetic energy of 8 GeV from the Booster accelerator. These protons are directed onto a beryllium target, resulting in the creation of hadrons (mostly pions): as a result of their decay, both ν_μ and ν_e neutrinos are generated. Any remaining particles are intercepted by a combination of concrete and steel absorbers. [1]

In addition to that, ICARUS is also interested by the off-axis neutrinos from NuMI[8] beam. BNB and NuMI produce very different beams, and the main differences between the two are spill duration and energy spectrum: NuMi has a shorter spill duration and an higher ν_e content. The data gathered using the NuMI beam will also be utilized for investigations extending beyond the Standard Model, as well as analyses pertaining to the dark sector. [3]

Physics goals

It is known that, in the Standard Model, neutrinos are neutral, left-handed and mass-less particles which only interact through weak interactions, described by CC and NC[9] interactions. They come in three flavors, one for each corresponding charged lepton (ν_e for electron, ν_μ for muon, ν_τ for tau). [4]

According to LEP[10], the number of active neutrinos (that is, neutrinos taking part to standard weak interactions) was determined to be $N_\nu \sim 3$. From studies of solar neutrinos and other studies, however, evidence of neutrino oscillation (and consequentially of the fact that neutrinos are not massless) has been found. The number of massive neutrinos can be larger than three, but there are also sterile neutrinos (that is, neutrinos not taking part to standard weak interactions). [4]

If neutrino have non-zero masses, a neutrino state of fixed flavor α, β can be written as a superposition of the neutrino mass eigenstates i, j that is

$$|\nu_\alpha\rangle = \sum_{i=1}^{N} U^*_{\alpha i} |\nu_i\rangle \qquad |\overline{\nu_\beta}\rangle = \sum_{j=1}^{N} U_{\beta j} |\overline{\nu_j}\rangle$$

[8] Neutrinos at the Main Injector
[9] Charged Current and Neutral Current
[10] Large Electron-Positron [Collider]

In the assumption of 3 massive neutrinos, the PMNS[11] matrix, or neutrino mixing matrix, U can be written in terms of three mixing angles θ_{12}, θ_{23}, θ_{31} and one Dirac-type CP phase δ (we are considering neutrinos as Dirac particles; in the case of Majorana mass terms, the mixing matrix contains two additional phases that have no any observable effect on neutrino oscillation). [4]

In the oscillation phenomenon, the flavour of a neutrino changes as it propagates through space and if we assume only two neutrino mixing (let's call them ν_α and ν_β) then the probability of a neutrino oscillating from flavour ν_α to flavour ν_β can be calculated as

$$P(\nu_\alpha \to \nu_\beta) = \sin^2(2\theta)\sin^2\left(1.267\frac{\Delta m^2 L}{E_\nu}\frac{[\mathrm{GeV}]}{[\mathrm{eV}^2][\mathrm{km}]}\right)$$

where $\theta = \theta_{12}$ is the mixing angle, $\Delta m = m_2^2 - m_1^2$ is the squared mass difference, L is the baseline length and E_ν is the neutrino energy.

In recent years, various experiments conducted at short baselines have observed anomalies, which if substantiated could suggest the existence of additional neutrino states: they can be categorized into two branches:

1. reactor anomalies, which involve a signal of neutrino disappearance at low energies emitted by nuclear reactors just a few meters from the source. This phenomenon may be attributed to uncertainties in the knowledge of reactor neutrino spectra and fluxes. A similar indication arises from experiments involving radioactive neutrino sources in Gallium, such as GALLEX[12] and SAGE[13]. This deficit may be accounted for by a model of ν_e disappearance, with $\Delta m^2 \geq 1\,\mathrm{eV}^2$;
2. anomalies found in LSND[14] and MiniBooNE[15] experiments. These observations reveal an excess of electron-like interactions involving both ν_μ and $\overline{\nu}_\mu$ produced by particle accelerators, which cannot be explained by the standard 3-neutrino model and implies oscillations occurring at a characteristic length-energy scale $L/E_\nu \sim 1\mathrm{m/MeV}$, with $\Delta m^2 \geq 1\,\mathrm{eV}^2$.

The prevailing interpretation of these anomalies leads to the hypothesis of the existence of an additional sterile neutrino, giving rise to a $3+1$ neutrino mixing model. Consequently, it is postulated that there exists a heavy neutrino ν_4 with a mass m_4, such that Δm^2_{41} falls within the range of $[0.1-10]\mathrm{eV}^2$ while m_1, m_2, m_3 are significantly smaller than m_4. Note that each anomaly could be explained by a $3+1$ model but no model so far is successful in fitting all experimental results at once. [1]

The SBN physics program aligns with this framework and was established to:

- understand the nature of MiniBooNE low energy excess, by exploiting MicroBooNE which uses a different technology and is supposed to understand if the excess is due to ν_e CC interactions;
- test for sterile neutrino (ν_4) hypothesis, both in appareance and disappareanche channels, using SBND as near detector and ICARUS as far detector. The use of the same detector technology will significantly diminish systematic errors, and the effective identification of ν_e by a LAr-TPC will aid in mitigating all backgrounds;
- lay the groundwork for future long-baseline experiments, such as DUNE[16], through the continued advancement of LAr-TPC technology and by conducting high-statistics measurements of ν-Ar cross sections in the few GeV range. [5]

LAr-TPC working principle

ICARUS, like the other two SBN detectors, is based on the LAr-TPC technology, proposed originally by Rubbia in 1977. It consists of TPCs filled with liquid Argon with remarkable tracking and calorimetric capabilities in the measurement of rare events, notably in the domain of neutrino interactions. [6]

During a neutrino-Argon interaction, illustrated in Fig. 2, the charged particles produced in neutrino interactions ionized and at the same time excite Argom atoms, which promptly undergo de-excitation emitting scintillation light. The quantity of scintillation photons generated is directly proportional to the energy deposited in the Argon. Consequently, by analyzing the collected charge, it becomes feasible to estimate the energy of the incident particle. [6]

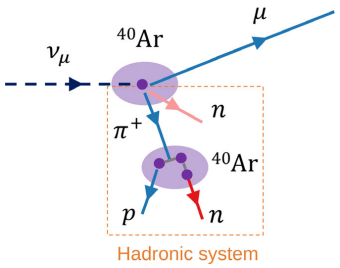

Fig. 2: A conceptual illustration of a ν_μ CC interaction with a ^{40}Ar nucleus, resulting in a μ and other products.

[11] Pontecorvo-Maki-Nakagawa-Sakata
[12] GALLium EXperiment
[13] Soviet–American Gallium Experiment
[14] Liquid Scintillator Neutrino Detector
[15] Mini Booster Neutrino Experiment
[16] Deep Underground Neutrino Experiment

The ionization process of Argon atoms involves the generation of Ar^+ and e^- pairs, which under the application of an electric field migrate towards the cathode and anode of the chamber. Fig 3 illustrates the structure of a LAr-TPC, composed of three key components:

- on one side, there exists a high-voltage cathode plane employed to establish a drift electric field throughout the chamber, typically $E_{\text{drift}} \sim 500\,\text{V}\,\text{cm}^{-1}$;
- on the opposing side, a set of three overlapped anode planes is positioned at a potential higher than the cathode. These planes consist of numerous parallel conducting wires with a few mm pitch. The orientation angle of the wires relative to the vertical varies from one plane to another;
- between the cathode and anode, a field cage is present, ensuring the uniformity of the drift field. This design minimizes deviations in drift electron trajectories from the shortest path between the point of ionization and the anode plane. [6]

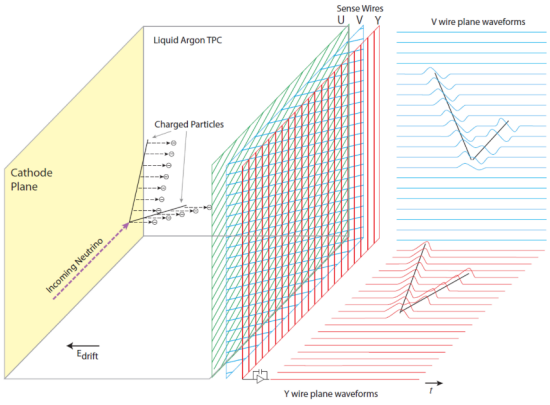

Fig. 3: An illustration of a neutrino-Argon interaction inside of a LAr-TPC. Ar^+ ions drift towards the cathode on the left and e^- drift towards the anode on the right. Signals get registered for every wire.

The inner planes, denoted as U and V in Fig. 3, function as induction planes since they are maintained at lower potentials, permitting drift electrons to pass through them and induce signals. Conversely, the outer plane, referred to as the collection plane (designated as Y in Figure 3), gathers the drift electrons on its wires. The angle information allows the reconstruction of spatial coordinates on the plane perpendicular to the drift direction. Additionally, by combining drift velocity information with data on time evolution, it becomes possible to reconstruct coordinates along the drift direction.

This advanced technology enables achieving a 3D spatial resolution down to the scale of mm^3. LAr-TPCs have been developed into detectors that merge this technology with calorimetric measurement and particle identification capabilities. This integration allows them to replicate the imaging capabilities of bubble chambers. Simultaneously, they are electronic and scalable, marking a significant advancement in detection systems. [6]

1.2 The ICARUS detector

The ICARUS T600 detector is the first large-scale LAr-TPC ever realized. Housed within its cryostats are 760 tons of liquid Ar, with an active mass of 476 tons and all maintained at a cryogenic temperature of 89 K.

Between 2010 and 2013, the detector successfully took data at the LNGS[17], recording cosmic rays and neutrinos from CNGS[18] beam. Following an extensive refurbishment period from 2015 to 2017 at CERN, the apparatus found its new home at Fermilab in the United States. Here, it serves as the far detector within the scope of the SBN project.

It is composed of a warm cryostat divided into two adjacent cold cryostats as it is shown in Fig. 4, known as the West Cryostat and East Cryostat with respect to the direction of the BNB.

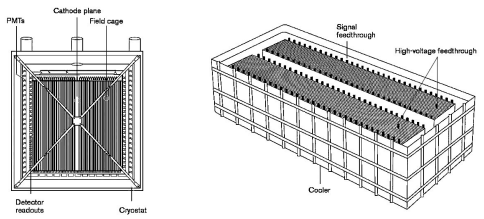

Fig. 4: Schematic of a cold cryostat. Each module hosts two TPCs separated by a common cathode.

Time Projection Chamber

In each module, two TPCs are housed, demarcated by a shared central cathode and encompassed within a liquid Argon volume subject to a drift field intensity of $E_{\text{drift}} \sim 500\,\text{V}\,\text{cm}^{-1}$. Under this field strength, the 1.5-meter separation between the cathode and anode planes results in a drift time of 1 ms. Due to the low transverse diffusion observed in LAr, ionization electron clouds produce distinct tracks on the anode surfaces.

The anode configuration within each TPC comprises three parallel wire planes, positioned 3 mm apart from one another, amounting to a total of 13312 wires for each TPC. These stainless steel wires have a 150 µm diameter and variable lengths upon their orientations.

[17] Gran Sasso National Laboratory
[18] CERN Neutrinos to Gran Sasso

Wires on each plane are oriented at 0°, 60°, −60° with respect to the horizontal axis. The coordinates of these wires on each plane are precisely determined, showing a remarkable resolution of 1 mm^3. This determination is achieved by amalgamating the ionizing event's temporal information with the wire coordinate. Through this process, an accurate three-dimensional reconstruction of the event becomes possible. [1]

Light Collection System

When a charged particle traverses the TPC, it can generate scintillation light through two mechanisms: the excitation of Argon atoms and the recombination of electron-ion pairs. These processes result in the formation of Ar_2^* molecules, which subsequently decay, emitting monochromatic VUV[19] photons with a wavelength $\lambda \sim 128$ nm. The emitted light exhibits two distinct decay components: a fast one with a lifetime $\tau \sim 6$ ns and a slow one with a lifetime $\tau \sim 1.5$ µs.

The detection system for scintillation light in ICARUS relies on 360 8-inch Hamamatsu R5912-MOD PMTs[20] positioned behind the wire chambers, deployed in groups of 90 devices behind each chamber. A wavelength shifter coating, converting VUV to visible light, is applied to the surface of each PMT window. This system ensures high sensitivity to ionizing events and provides precise timing information for each interaction with resolutions on the order of nanoseconds. [1]

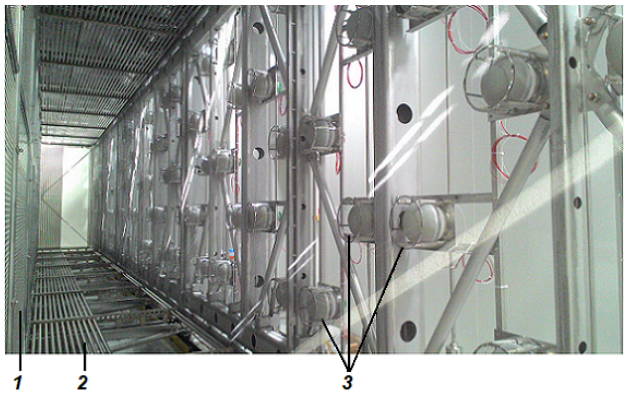

Fig. 5: An internal view of one of the four ICARUS T600 drift volumes, showing (1) the cathode, (2) the field-shaping electrodes, and (3) the array of PMTs utilized for detecting scintillation light. [7]

The light collection system involves saving and utilizing PMT waveforms for timing, calorimetry, and triggering purposes. For each TPC, 90 PMTs are linked to sets of 6 CAEN V1730B digitizer boards, each equipped with 16 channels, with the last channel serving other functions. These boards sample PMT signals at a rate of 500 MS/s with a 14-bit resolution. Each signal is discriminated using a threshold of 400 ADC (∼13 pe[21]) to generate a series of LVDS[22] output signals, representing logic-OR combinations of adjacent 2 by 2 PMTs. The output signals from each TPC undergo processing by a NI-PXIe 7820 FPGA, one per T300 module, equipped with programmable logic.

Cosmic Ray Tagger

The ICARUS T600 detector at Fermilab operates at shallow depth (3 m concrete overburden), constantly exposed to significant cosmic ray activity. This constitutes the primary source of background for various physics analyses. These cosmic rays, if not properly identified, could be mistaken for part of a neutrino interaction. To mitigate this issue, a dedicated CRT[23] system was developed. This completely encloses the detector and identifies cosmic muons, effectively separating them from genuine neutrino interactions.

The CRT system is constructed using plastic scintillator modules, organized into three sub-systems covering the top, side, bottom regions of the detector, as it can be seen from Fig. 6. Scintillators are equipped with SiPM[24] for readout, except for the bottom system that utilizes PMTs. This system has been fully installed and is actively collecting data, ensuring accurate discrimination between cosmic ray events and neutrino interactions. [1]

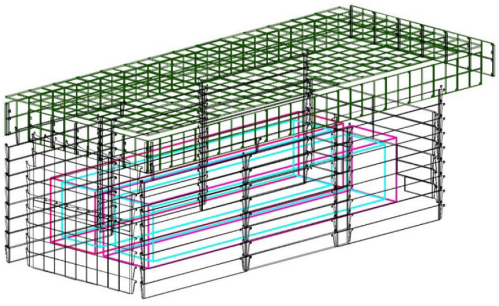

Fig. 6: Diagram illustrating the ICARUS T600 Cosmic Ray Tagger system, divided into three segments (top, side, bottom), each of which made with plastic scintillators with slight design variations.

[19] Vacuum UltraViolet
[20] PhotoMultiplier Tubes
[21] photoelectrons
[22] Low Voltage Differential Signaling
[23] Cosmic Ray Tagger
[24] Silicon PhotoMultipliers

2 ICARUS Trigger System

The ICARUS detector is interested by an event rate of $\sim 0.29\,\text{Hz}$ within the beam gates, equivalent to ~ 23000 events daily. This rate arises from:

- BNB events rate (with a spill duration of $1.6\,\mu\text{s}$ and 5×10^{12} protons per spill at $\sim 4\,\text{Hz}$ repetition rate), which includes a neutrino interaction every ~ 180 spills, a similar rate for beam-associated events and a cosmic event every ~ 55 spills, resulting in 1 event every ~ 35 spills or a rate of $\sim 0.14\,\text{Hz}$;
- NuMI events rate (with a spill duration of $9.5\,\mu\text{s}$ and 6×10^{13} protons per spill at $\sim 0.75\,\text{Hz}$ repetition rate) which includes a neutrino interaction every ~ 53 spills and a cosmic event every ~ 7 spills, resulting in 1 event every ~ 6 spills or a rate of $\sim 0.12\,\text{Hz}$;
- background due to Ar^{39} decays, to additional events generated in the decay of cosmic muons crossing the detector in those few µs before proton extractions, and random triggers, resulting in a rate of $\sim 0.03\,\text{Hz}$

To handle this substantial volume of data, starting from the initial 5 Hz beam gates rate, a multilevel trigger system is essential. This system is tasked with managing the data influx and selecting the relevant physical events. An additional offline step is then performed to further process the data and associate these events with genuine neutrino interactions. [8]

2.1 Trigger types

When the trigger primitive aligns temporally with the beam gate, it results in the production of a global trigger. In this case, gate signals are synchronized with the beam spills to match the regions of significant physics activity (and thus are slightly longer than the actual duration of the beam spills), and PMT waveforms are recorded within a $28\,\mu\text{s}$ interval around the trigger time to fully cover the spill region. When a global trigger occurs, readout process for various detector subsystems, including TPCs (for 1.5 ms, aligning with the e^- drift time), PMTs, and CRTs, is activated. Data are recorded in both cryostats, even if the triggering light is visible only on one cryostat.

There are also local triggers or "out-of-time triggers": these triggers employ shorter $10\,\mu\text{s}$-long acquisition windows for PMT waveforms and are activated by primitive occurring outside of the beam spill and within a 2 ms window around the global trigger. This setup is useful as it allows the recording of all scintillation light associated with cosmic ray activity during the TPC drift time, a crucial step for cosmic background rejection.

Majority Trigger

The majority trigger serves as the standard triggering system for the ICARUS detector and relies on a majority logic approach to generate the PMT trigger primitive. To achieve this, each cryostat is segmented into three 6-meter-long windows, each containing 60 PMTs (30 on the West TPC and 30 on the East TPC). For the generation of a global majority trigger primitive, at least 5 LVDS signals within one of these windows are required, while for the generation of a local majority trigger primitive at least 9 LVDS signals are required.

MinBias Triggers

Simultaneously, in certain scenarios, there is a need not to enforce any requirement on the coincidence of light but only necessitate the presence of a gate. This condition applies to the MinBias trigger. In this specific trigger type, there is no bias introduced by mandating PMT signals to initiate a trigger. This approach can be implemented both synchronously with the beam and independently off-beam. It's important to note that for a single beam gate, this type of trigger cannot be utilized in conjunction with the majority trigger.

Events captured through a MinBias trigger serve various purposes, including timing assessments during detector activation, simulation studies, and establishing an unbiased data sample for trigger efficiency analyses. Off-beam triggers are often used for calibration tests.

2.2 Hardware implementation

The trigger system layout is built upon NI[25] PXIe[26]. Within a single NI-1082 PXIe crate, there resides an NI PXIe-8840 RTC[27], one SPEXI board by INCAA Computers, and three NI PXIe-7820R FPGAs.

The SPEXI board obtains information about neutrino beam extraction from both BNB and NuMI through the White Rabbit network. It then generates a 66.6 MHz clock for the PMT digitizers; TT-Link trigger and clock signals for the TPC digitizers; a 2 ms-wide beam enable

[25] National Instruments
[26] PCI eXtensions for Instrumentation express
[27] Real-Time Controller

signal, enabling PMT readout; a 1.6 µs-wide (for BNB, 9.5 µs-wide for NuMI) beam gate enable signal. Two of the three FPGAs are specifically allocated for PMT trigger functions in each cryostats. These FPGAs assess the number of LVDS signals surpassing the threshold and apply the majority logic rule. In the presence of a global trigger, the DAQ[28] system initiates the readout process for the entire detector. Simultaneously, the RTC retrieves timestamps for the beam gate and global triggers from the SPEXI board. It then transfers this timestamp data to the DAQ system using the TCP/IP[29] transfer protocol.

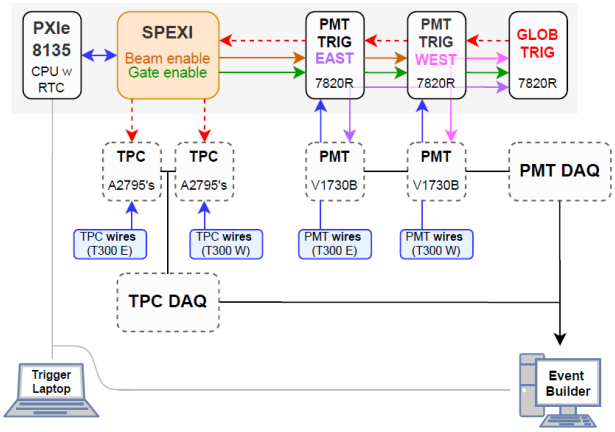

Fig. 7: Illustration of the trigger configuration, including the PXIe Real-Time Controller, the SPEXI board, and the three FPGAs utilized for trigger management.

2.3 Adder Trigger System

Recent comprehensive studies on global trigger efficiency, conducted using both Monte Carlo simulations and collected data, have indicated an efficiency of ∼97% for CC events with deposited energies greater than 300 MeV. However, hints of reduced efficiency were observed in the detection of cosmic rays, specifically for out-of-time PMT triggers, and there could be interest in improving efficiency for NC events or for CC events below 300 MeV. The current trigger electronics rely on discriminating individual PMT signals and utilizing majority patterns. This approach might be enhanced by integrating a system based on adder boards.

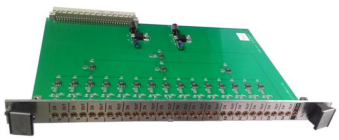

Fig. 8: Picture of an adder board.

[28] Data Acquisition
[29] Transmission Control Protocol/Internet Protocol

Adder boards

Each custom-made board comprises 2 stages, depicted in Fig. 9. The initial stage functions as a signal splitter, designed to receive 15 PMT signals as inputs. This stage leaves almost unaffected the PMT signals' line to the digitizers, retaining 95% amplitude on a 50 Ω impedance while scaling each signal by a factor of 5% (one more time, on a 50 Ω impedance), which then undergoes shaping through a Sallen-Key filter with a 20 ns shaping constant. Subsequently, the adder stage performs the analog sum of the 15 scaled PMT signals.

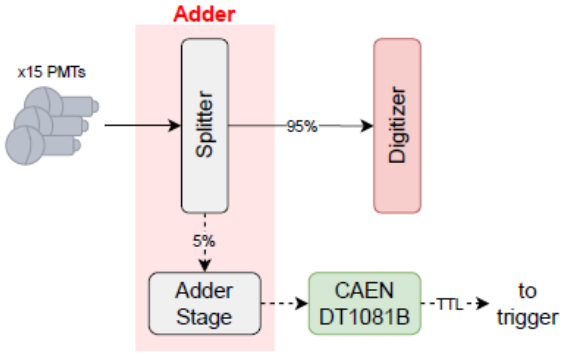

Fig. 9: Illustration of the adder trigger system setup. Starting from the left: the 15 PMT signals are divided into two parts with 95% and 5% components. The former proceeds to the digitizer, while the adder stage combines the 15 signals scaled by 5%. Finally, an external module is employed for discrimination.

Each analog sum is then subjected to discrimination via a CAEN DT1081B Programmable Logic Unit—each T300 module is equipped with one. This module performs all the necessary processing tasks for the output lines, including discrimination, TTL conversion, counting, and more. It is essential to note that the discrimination threshold needs precise tuning to optimize detection efficiency. The ultimate output, in TTL format, becomes part of the trigger logic for further signal processing via FPGA and for generating the global trigger.

Motivation

The output from the discriminated adders serves as an additional source of trigger information, offering several advantages. Firstly, adders provide supplementary details about the light yield, which is totally independent of the majority logic. Secondarily, in scenarios with low detector occupancy (for example a cosmic track near the detector corners), a substantial amount of light may be collected by only a few PMTs. By triggering on the sum, the constraint on the number of activated PMTs

is eliminated. Furthermore, this trigger system can be employed in conjunction with the majority trigger, increasing global trigger efficiency for events below 300 MeV for CC events and in general for NC events. It is also valuable for assessing the relative trigger efficiency of the majority logic, enabling real-time monitoring of its performance.

Objectives

This research project explores the implementation of an adder-based trigger system. The main goals include studying the adder trigger rate to determine the optimal threshold range, quantifying the contribution of the adder-based trigger system to the overall efficiency, computing the standalone adder efficiency on an unbiased sample and implementing software emulation for adder trigger, starting from single PMT waveforms and analyzing adder waveform to check if emulation performs well. More specifically, this internship report is focused on the first two tasks, which is the study of adder trigger rate and the study of tracks undetected by majority-5 but captured by adder trigger system.

3 Analysis of adder trigger rate

This analysis focused on the study of trigger rate from adder boards holds significant importance for several reasons: it is crucial to verify the stability of the adder trigger rate over time and to ensure that it aligns with the expected trend based on the threshold employed.

Data were collected using two distinct configurations: one triggered on the corner adders, the other one utilized instead the central adders for triggering. The difference between the two setups can be seen in Fig. 10.

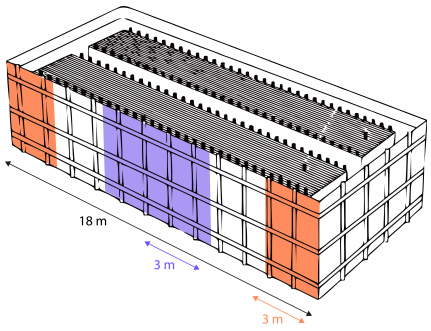

Fig. 10: Details of a cryostat module, revealing its segmentation into three 6-meter-long windows, each hosting 30 PMTs on both the west and east sides. In the above illustration, red denotes the corner adder boards, whereas blue indicates the central adder boards (each board processes the signal of 15 PMTs).

Analysis of the adder trigger rate has therefore been performed separately for the two data sets, processing both results for the corner adders setup and the central adders setup. Furthermore, for each configuration, individual analyses have been conducted for events from BNB and events from NuMI. It's important to acknowledge that, during the summer beam shutdown, no physical beam was present. In this scenario, the different acquisition windows were emulated, and the triggered events consisted mainly of cosmic rays.

3.1 Stability of trigger rate

In order to ensure there are no anomalous fluctuations, it is essential to verify the stability of the trigger rate from the adder boards. Once chosen an arbitrary time range of $T = 20\,\text{min}$, trigger rate has been estimated as the number of triggers happened in the time range T, over T, and then plotted as it can be seen from Fig. 11.

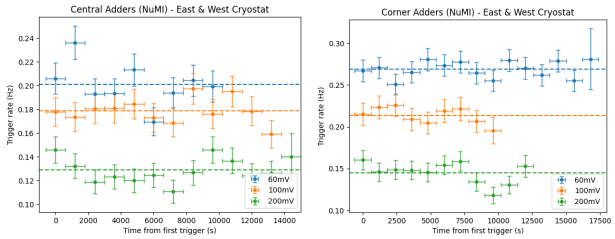

Fig. 11: Plots showing trigger time in function of time, for the central-corner adders configuration and for three different values of threshold (namely 60, 100, 200 mV). Error on time is half of T, error on rate is poissonian.

3.2 Relationship rate-threshold

After confirming the stability of the adder trigger rate over time, it becomes feasible to plot the rate in function the threshold to verify if it aligns with the theoretical. The expected pattern entails an exponential decrease in the rate in function the threshold. The three values of threshold - 60, 100, 200 mV - have been chosen in an optimal range (not too low, since it might be unmanageable from the point of view of DAQ, and not too high, since it would lead to a minimum rate).

Characterization of each cryostat

It is possible to calculate the mean trigger rate over the entire duration for each configuration and threshold value. This enables the plotting of rates over the thresh-

old. Besides displaying the total trigger rate, which considers both the east and west cryostat modules, it is also possible to depict the trigger rate of each cryostat module. This approach allows for a detailed characterization of each module and an example is shown in Fig. 12.

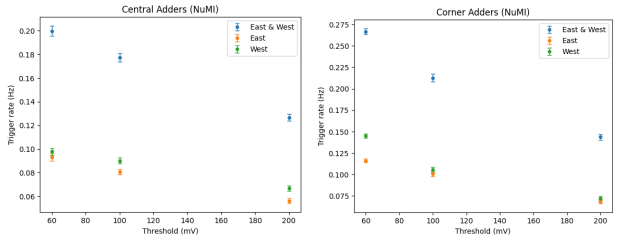

Fig. 12: Plots showing trigger rate in function of threshold, for NuMI-like gates, in the central-corner adder setups. Threshold values are nominal and considered as errorless, while error on rate is still poissonian.

Characterization of each module allows to see that west cryostat has an higher trigger rate from adder boards than east cryostat: an evident asimmetry, probably due to the structural differences between the two modules.

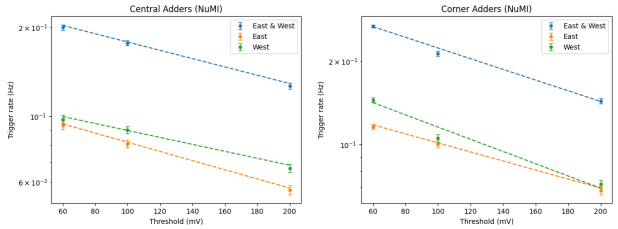

Fig. 13: Log scale plots showing trigger rate in function of threshold, for NuMI-like gates, in the central-corner adder setups. A linear fit has been shown to verify that this trend match with the exponential model.

From Fig. 12 it is clear that the trend matches with the theoretical model; the double-check performed through a log scale plot as the one in Fig. 13 confirms this result.

Characterization of each board

The data storage method enables precise identification of the board(s) triggering a specific event. This information allows for the calculation of the trigger rate for each adder board, facilitating thus the characterization of individual boards, as it can be seen in Fig. 14.

The characterization of each board reveals that when comparing the total rate of the cryostat with the sum of the rates for each of the four boards, the latter is higher than the former. This discrepancy is attributed to multiple triggers, meaning events triggered by more than one board.

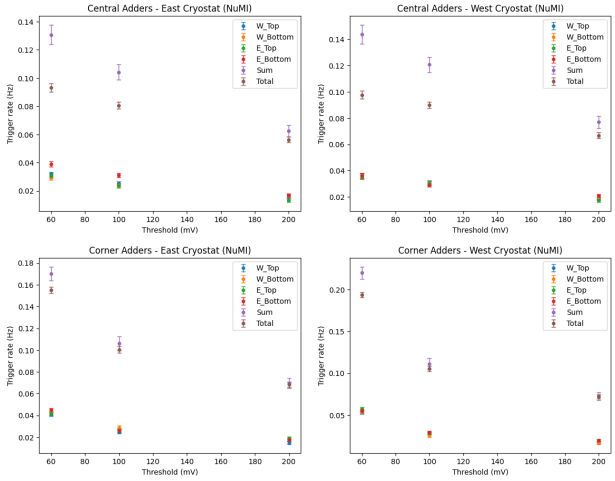

Fig. 14: Plots showing trigger rate in function of threshold, for NuMI-like gates. Upper plots refer to the central adders setup, lower plots refer instead to the corner adders. Together with the trigger rate for each board, it is also plotted the total rate of cryostat (brown) and the sum of the four rates for each board (purple).

Upon calculating the contribution of these multiple triggers to the total rate, as shown in Table 2, it becomes evident that this contribution is significantly higher in the central adders compared to the corner adders. In the corner regions, multiple triggers can only occur between the two northern adders or the two southern adders, due to the cathode transparency. In the central regions, multiple triggers can occur between both the two northern or two southern adders, as well as between a northern and a southern adder, given their adjacent positions.

		60 mV	100 mV	200 mV
central adders	**east**	40%	29%	11%
	west	47%	34%	15%
corner adders	**east**	10%	5%	2%
	west	14%	5%	1%

Table 2: Percentage contribute of multiple triggers to the total rate, for NuMI-like gates, both for central and corner adders setup.

4 Incremental performance of adders for 'neutrino-like' events

This study aims to assess the usefulness of the adder-based trigger system with respect to the majority trigger, in particular for events that resemble neutrino in-

teractions as much as possible starting from the available data set of cosmic rays events.

To achieve this goal, cosmic-ray data taken with a trigger generated by the central adder boards were analyzed. Particles exhibiting a topology closely similar to neutrino-Argon charged current interactions were identified as stopping muons and muon decays, i.e. muons that enter the detector and lose all the energy within the detector without exiting, by either capturing an Argon atom or decaying into a Michel electron and two neutrinos. For these events the response of the majority-based trigger was emulated via software based on the collected PMT waveforms, to verify if the adder trigger was providing any improvement.

4.1 Selection of neutrino-like events

The initial step involved the development of an algorithm to identify these kinds of interaction, referred to as "neutrino-like events". To accomplish this, the following selection cuts were applied:

1. both the starting and the ending points of each track must be within 5 cm of the fiducial volume;
2. track length must be greater than 30 cm;
3. the $\mathrm{d}Q/\mathrm{d}r$ profile must exhibit the Bragg peak i.e. an increase in the ionization, occurring just before the particle comes to rest.

Before applying the selection cuts, a two-dimensional distribution of starting and ending points was plotted. These plots aimed to verify whether most points fell within the fiducial volume and simultaneously confirm the accuracy of the nominal fiducial coordinates, as it can be seen in Fig. 15.

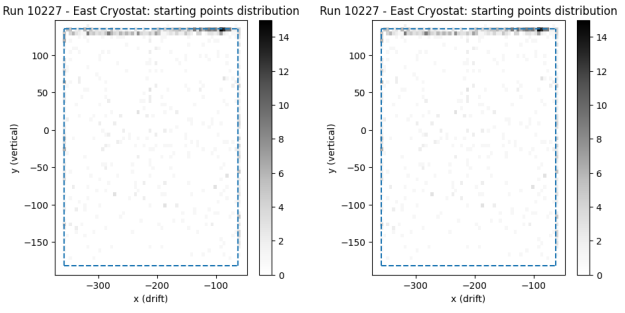

Fig. 15: Plots showing 2D distribution of starting and ending points in the East Cryostat, projected on the xy plane. These data refer to the run taken with a threshold of 200 mV; the same analysis was performed for the other thresholds, and also with respect to the z axis.

After applying the first two selection cuts, it is interesting to examine whether the tracks selected so far follow the expected length and angular distribution. The length distribution is supposed to show an exponential decrease with the length, while the angular distribution should be isotropic as regards the drift and beam direction and anisotropic as regards the vertical direction, given that cosmic rays primarily come from above.

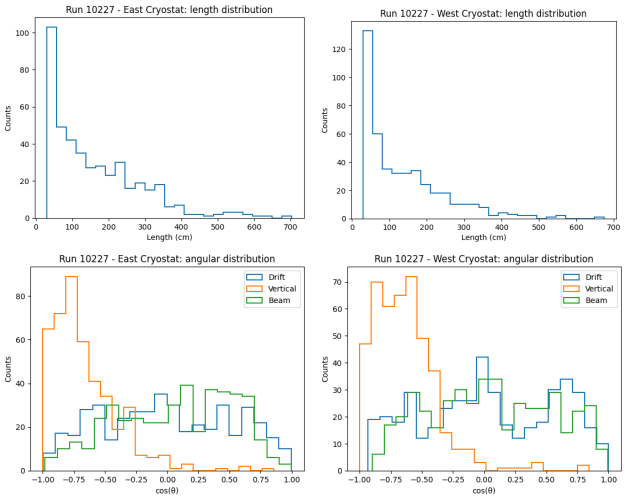

Fig. 16: Plots showing length and angular distributions in the East and West Cryostats. These data refer to the run taken with a 200 mV threshold; the same analysis for the other thresholds gave the same results.

Once performed all these checks, the analysis advanced to the selection of tracks showing a Bragg peak in their $\mathrm{d}Q/\mathrm{d}r$ profile. As this peak typically occurs before the particle stops, the requirement set for the tracks was that the mean $\mathrm{d}Q/\mathrm{d}r$ value in the last 5 cm of the track must exceed two times the most probable $\mathrm{d}Q/\mathrm{d}r$ value. The latter was exctracted from the fit of the $\mathrm{d}Q/\mathrm{d}r$ distribution using a convolution of Gaussian and Landau.

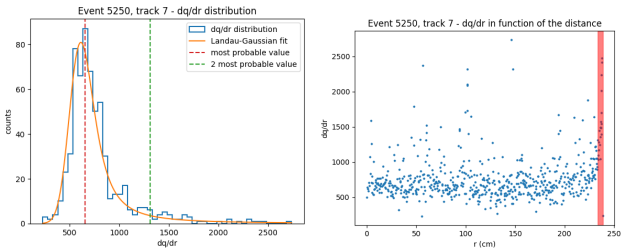

Fig. 17: Plots showing $\mathrm{d}Q/\mathrm{d}r$ distribution and profile of an event in the West Cryostat, for the run taken with a threshold of 200 mV. In the right plot, the red bar indicates the last 5 cm of the track and in fact the Bragg peak is quite evident.

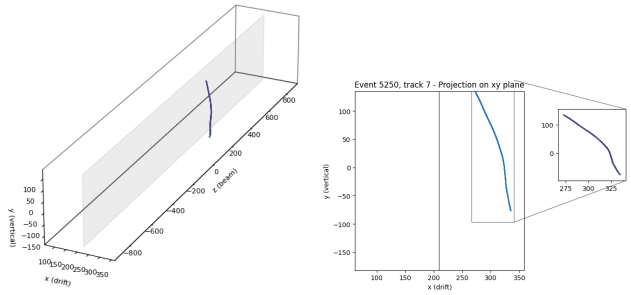

Fig. 18: Plots showing 3D and 2D display of the event of Fig. 17, from which it is evidently interpretable as a stopping muon.

4.2 Conditional efficiency

Running the software emulation of a majority-5 trigger on the selected events, it was found that $\sim 98\%$ of the events both triggered by the majority trigger and the adder-based trigger. Fig. 19 and 20 show the only event, among the 48 selected, which was not triggered by majority-5.

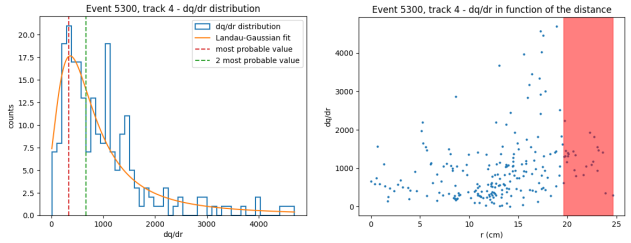

Fig. 19: Plots showing $\mathrm{d}Q/\mathrm{d}r$ distribution and profile of an event in the East Cryostat, for the run taken with a threshold of 200 mV. In the right plot, the red bar indicates the last 5 cm of the track; in this plot the Bragg peak is not so evident.

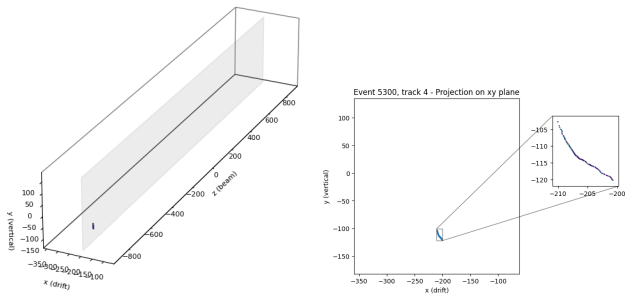

Fig. 20: Plots showing 3D and 2D display of the event of Fig. 19.

From Fig. 20 it is evident that this event has a short track and probably for this it did not trigger majority-5.

Conclusions

During the first part of this internship project, the adder board trigger rate has been studied. It has been checked that trigger rates of adder boars are stable in time and follow the expected trend in function of the threshold used, which are within an optimal range. Through the characterization of each cryostat, it has been observed that West Cryostat has an higher trigger rate than East Cryostat; through the characterization of each adder board, it has been observed the existence of multiple triggers, qualifying and quantifying them separately for the two cryostats.

In the second part of the project, a conditional study of the inefficiency of the majority trigger compared to the adder trigger was performed on a sample of neutrino-like events. It was observed that an adder-based trigger system can improve majority-5 trigger system by $\sim 2\%$.

Regarding future developments of this work, it might be interesting to investigate how this trigger system behaves for CC interactions below 300 MeV and for NC interactions, in order to keep improving the global trigger efficiency and to be able to implement the adder-based trigger system together with the majority trigger system.

Acknowledgements I would like to express my sincere gratitude to the Organizing Committee of the Italian Student Program at Fermilab, including Giorgio Bellettini, Simone Donati and Emanuela Barzi, for providing me with the invaluable opportunity to participate. Your selection has been an honor and a pivotal moment in my academic journey.

I am deeply grateful to my supervisors Angela Fava and Donatella Torretta, whose guidance, expertise, and unwavering support have been instrumental in shaping this project. Your mentorship has not only enriched my understanding but also inspired me to achieve more than I thought possible.

I want to express a special appreciation to Riccardo Triozzi and Jacob Zettlemoyer for their generous assistance and support. Their insights and advice have been invaluable, and I am grateful for their willingness to share their expertise.

I extend my heartfelt appreciation to the ICARUS Collaboration for fostering an environment of collaborative research and discovery. The collective efforts and shared knowledge within the collaboration have undoubtedly contributed to the success of this endeavor.

To all those who have played a role, big or small, in this journey, I am truly thankful. Your contributions have left an indelible mark on my academic and personal growth.

References

1. R. Triozzi, "Studies of the trigger performance of the ICARUS T600 detector at Fermilab," 2022.
2. A. Szelc, M. Antonello, and J. Pater, "A Proposal for a Three Detector Short-Baseline Neutrino Oscillation Program in the Fermilab Booster Neutrino Beam," *ArXiv*, 2015.
3. S. E. Kopp, "The NuMI Neutrino Beam at Fermilab," vol. 773, pp. 276–278, 6 2005.
4. G. Bellini, L. Ludhova, G. Ranucci, and F. Villante, "Neutrino Oscillations," *Advances in High Energy Physics*, vol. 2014, 01 2014.
5. M. Bonesini, "The Short Baseline Neutrino Program at Fermilab," 03 2022, p. 009.
6. M. Diwan, M. Potekhin, B. Viren, X. Qian, and C. Zhang, "A novel method for event reconstruction in Liquid Argon Time Projection Chamber," *Journal of Physics: Conference Series*, vol. 762, p. 012033, 10 2016.
7. K. Majumdar and K. Mavrokoridis, "Review of Liquid Argon Detector Technologies in the Neutrino Sector," *Applied Sciences*, vol. 11, p. 2455, 03 2021.
8. Babicz, Marta, "ICARUS T600 Trigger Study at the Short-Baseline Neutrino Experiment." [Online]. Available: https://indico.cern.ch/event/864614/contributions/3859763/attachments/2038762/3413897/EPNU_talk.pdf